Proceedings of the IDETC/CIE 2011
ASME International Design Engineering Technical Conferences &
Computers and Information in Engineering Conference
August 28-31, 2011, Washington, DC, USA

DETC2011-48770

TERRAMECHANICS MODELING OF MARS SURFACE EXPLORATION ROVERS FOR SIMULATION AND PARAMETER ESTIMATION

Karl Iagnemma
Massachusetts Institute of Technology
Cambridge, MA, USA

Carmine Senatore
Massachusetts Institute of Technology
Cambridge, MA, USA

Brian Trease
Caltech / JPL
Pasadena, CA, USA

Raymond Arvidson
Washington University
St. Louis, MO, USA

Keith Bennett
Washington University
St. Louis, MO, USA

Amy Shaw
Washington University
St. Louis, MO, USA

Feng Zhou
Washington University
St. Louis, MO, USA

Lauren Van Dyke
Washington University
St. Louis, MO, USA

Randel Lindemann
Caltech / JPL
Pasadena, CA, USA

ABSTRACT

In 1997 and 2004, small wheeled robots ("rovers") landed on the surface of Mars to conduct scientific experiments focused on understanding the planet's climate history, surface geology, and potential for past or present life. Recently, the Mars Exploration Rover (MER) "Spirit" became deeply embedded in regolith at a site called Troy, ending its mission as a mobile science platform. The difficulty faced in navigating mobile robots over sloped, rocky, and deformable terrain has highlighted the importance of developing accurate simulation tools for use in a predictive mobility modeling capacity. These simulation tools require accurate knowledge of terrain model parameters. This paper describes a terramechanics-based tool for simulation of rover mobility. It also describes ongoing work toward estimation of terrain parameters of Mars soil.

1.0 INTRODUCTION

In 1997 and 2004, small wheeled robots ("rovers") landed on the surface of Mars to conduct scientific experiments focused on understanding the planet's climate history, surface geology, and potential for past or present life. These NASA/JPL rovers were expected to negotiate loose, sloped, and rocky terrain to access scientifically interesting sites. The 1997 Sojourner rover limited its traverses to relatively short distances (i.e. a few meters) through flat, rocky terrain under close human supervision [1]. The 2004 twin Mars Exploration Rovers (dubbed "Spirit" and "Opportunity") have performed longer-distance traverses through soil-covered, sloped terrain, with some autonomous operation [2]. However, the MER rovers have experienced numerous instances of severe sinkage and wheel slip in highly deformable soil. In fact, Spirit became deeply embedded in soil after breaking though a soil crust. This was in part due to a failed right front wheel actuator, which made mobility and extrication very difficult [3]. Opportunity has also encountered mobility challenges with high wheel sinkage and associated slip when crossing wind-blown ripples [4].

The difficulty faced in navigating mobile robots with complex drive dynamics over sloped terrains covered by a mix of rock exposures and deformable soils has highlighted the importance of developing accurate simulation tools for use in a predictive mobility modeling capacity. This is particularly true because Opportunity is headed toward the rim of Endeavour, a 20 km wide ancient crater. The rover will need to traverse 10 to 15 degree slopes covered with deformable soils to reach the outcrops that expose what the science team believes are clay minerals formed in an early, wet Martian environment.

This paper describes recent work toward developing a terramechanics-based model of rover mobility on planetary surfaces. The resulting simulation tool, ARTEMIS (Adams-based Rover Terramechanics and Mobility Interaction Simulator), is composed of a 200-element MSC-Adams dynamic rover model, a library of terramechanics subroutines, and high-resolution digital elevation maps of the Mars surface.

Rover-terrain interactions that are modeled include longitudinal, lateral, and vertical wheel-terrain interaction forces, the effect of slip sinkage, and multipass effects. (Refer to a companion paper at this conference for a more detailed description of ARTEMIS [5]). The model will be employed to help plan drives for Opportunity on Endeavour's rim, providing a set of outputs to help engineers choose routes to desired rock targets that minimize wheel sinkage and slip, and thus reduce the probability of embedding Opportunity.

To ensure accurate model predictions, ARTEMIS requires knowledge of terrain model parameters. For terrestrial applications, terrain model parameter estimation typically requires analyzing soil samples via standard geoengineering methods such as triaxial testing and direct shear testing. Since Mars regolith samples are not available for direct testing, other parameter estimation methods must be adopted. Previous researchers have developed methods for terrain parameter estimation based on model-based observers [6-9]. These methods typically employ simplified wheel-terrain interaction models to facilitate efficient, recursive, linear observer formulation. Here, an approach to parameter estimation is described that merges nonlinear terramechanics models with Spirit rover telemetry in a constrained optimization framework.

2.0 ARTEMIS TERRAMECHANICS MODEL

ARTEMIS has been developed using MSC-Adams multibody dynamics simulation software for the purpose of analyzing MER rover mobility. A key component of ARTEMIS is its terramechanics model. This model is described here.

2.1 Force Modeling

ARTEMIS relies on terramechanics relations first developed by Bekker [10] and later modified by Wong [11]. Figure 1 indicates the chosen coordinate frame, introduces the stresses acting on the wheel, and presents the orientation of the wheel with respect to the local slope.

The normal stress at the wheel-terrain contact patch is assumed to be purely radial, and is calculated using the Bekker-Wong equation [11-13]:

$$\sigma = \begin{cases} \sigma_1 = \left(\frac{k_c}{b} + k_\phi\right) z_1^n & \theta_m < \theta < \theta_f \\ \sigma_2 = \left(\frac{k_c}{b} + k_\phi\right) z_2^n & \theta_r < \theta < \theta_m \end{cases} \quad (1)$$

$$z_1 = r\left(\cos\theta - \cos\theta_f\right)$$

$$z_2 = r\left(\cos\left(\theta_f - \frac{\theta-\theta_r}{\theta_m-\theta_r}\left(\theta_f-\theta_m\right)\right) - \cos\theta_f\right)$$

where θ_f is the soil entry angle, θ_r is the exit angle, and θ_m is the angle at which the maximum normal stress occurs (see Figure 1). Parameters k_c, k_ϕ, n depend on soil properties, r and b correspond to the wheel radius and width, respectively. The angle at which the maximum normal stress occurs can be calculated as:

$$\theta_m = (a_1 + a_2 i)\theta_f \quad (2)$$

The wheel is divided into "slices" normal to the axis of rotation (see Figure 1) and the entry and exit angle are calculated for each slice. The normal stress in each patch is computed independently.

Shear stress in the longitudinal direction (i.e. the direction of travel) is the primary source of driving traction [14]. Shear stress is function of soil parameters and the measured shear deformation, *j:*

$$\tau_x = (c + \sigma \cdot \tan\phi)\left(1 - e^{-\frac{j_x}{k_x}}\right) \quad (3)$$

$$j_x = \int_0^{t_0} v_t dt = \int_\theta^{\theta_f} v_t \frac{d\theta}{\omega} \quad (4)$$

where v_t is the tangential slip velocity and k_x is the shear modulus. Integrating j_x over the wheel-terrain geometry and

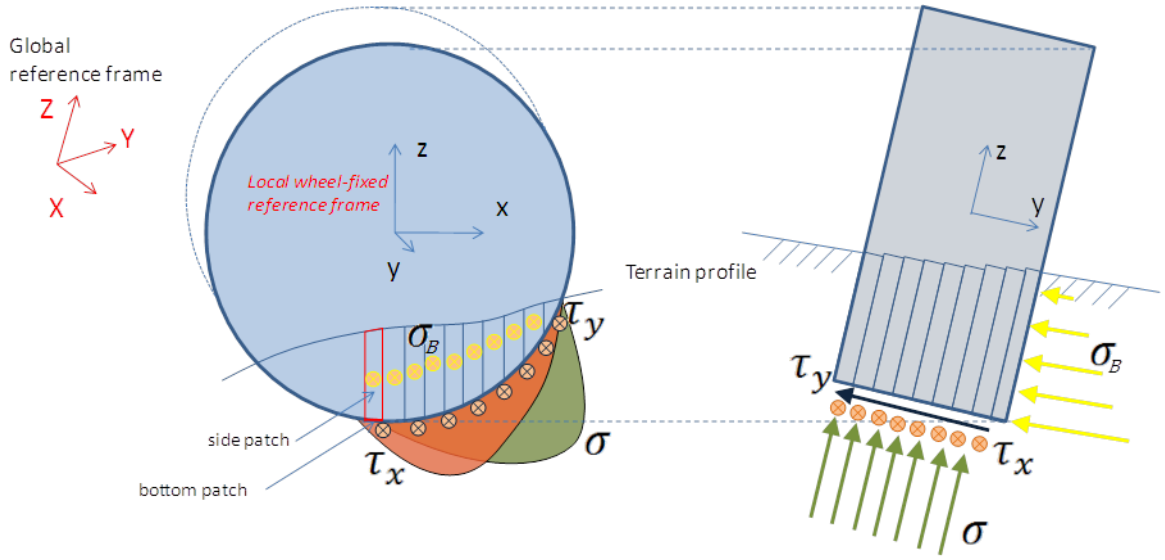

Figure 1: Coordinate frame and representation of wheel and soil for terramechanics analysis

considering the slip definition given in Equation 21 yields:

$$\text{Driving:} \quad j_x = r\left(\theta_f - \theta - (1-i)\left(\sin\theta_f - \sin\theta\right)\right)$$
$$\text{Braking:} \quad j_x = r\left(\theta_f - \theta - \frac{\left(\sin\theta_f - \sin\theta\right)}{i+1}\right) \tag{5}$$

Forces in the lateral direction of each wheel are the result of lateral shear stresses, which are calculated in a similar fashion to the longitudinal shear stresses [14,15]

$$\tau_y = (c + \sigma \cdot \tan\phi)\left(1 - e^{-\frac{j_y}{k_y}}\right) \tag{6}$$

$$j_y = \int_0^{t_0} v_y dt \tag{7}$$

where v_y is the lateral velocity of the wheel, depicted in Figure 2.

$$v_y = v_x \tan\beta \tag{8}$$

Integration of Equation 7 leads to closed-form equations for j_y for slip (driving) and skid (braking) conditions.

$$\text{Driving:} \quad j_y = r(1-i)\left(\theta_f - \theta\right)\tan\beta \tag{9}$$

$$\text{Braking:} \quad j_y = \frac{r(\theta_f - \theta)\tan\beta}{(1+i)} \tag{10}$$

Shear calculations are performed on discrete "patches" of the wheel mesh and are then summed to provide a single set of forces at the wheel center.

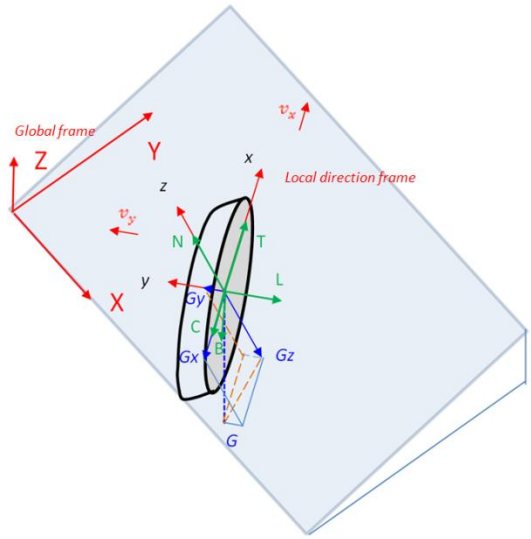

Figure 2: Local (*xyz*) and global (*XYZ*) coordinates in ARTEMIS

Integration of Equation 6 along the contact patch profile leads to a lateral force component due to shearing action.

$$F_u = br\int_{\theta_r}^{\theta_f}(c + \sigma(\theta)\tan\theta)\left(1 - e^{-\frac{j_y}{k_y}}\right)d\theta \tag{11}$$

Bulldozing forces are computed only in the lateral direction (i.e. on the wheel side walls). These bulldozing forces are modeled as a flat cutting blade moving through soil. The solutions of the cutting blade problem are based on Terzaghi's solution for soil bearing capacity [17]. The basis for calculation is shown in Equations 12 and 13, where Terzaghi's equation is presented.

$$\sigma_B = \gamma z N_\gamma + cN_c + qN_q \tag{12}$$

$$N_\gamma = \frac{2\left(N_q+1\right)\tan\phi}{1+0.4\,\sin 4\phi} \quad N_c = \frac{N_q - 1}{\tan\phi} \quad N_q = \frac{e^{(1.5\pi-\phi)\tan\phi}}{2\cos^2(\pi/4+\phi/2)} \tag{13}$$

Integrating the predicted stress distribution along the tire sidewall leads to the calculation of lateral force due to bulldozing:

$$F_b = \int_{-r\sin\theta_f}^{r\sin\theta_f}[\gamma N_\gamma f(x) + cN_c + qN_q]f(x)dx \tag{14}$$

where $f(x) = \left(\sqrt{r^2 - x^2} - z_0\right)$.

The effect of the MER wheel grousers (cleats) on traction was also modeled. The force acting on each grouser (F_g) is given by Equation 15 and depicted in Figure 3.

$$F_g = b\left[\frac{1}{2}\gamma h_g^2 N_\phi + 2ch_g\sqrt{N_\phi}\right]\cos\alpha \tag{15}$$

where $N_\phi = \tan^2(\pi/4 + \phi/2)$. Grouser influence is modeled after Terzaghi's bearing capacity equation, where h_g is the height of the grouser and α is the grouser angle. The force acting on each grouser is decomposed into two directions according to the center angle θ. To calculate torque, the net grouser force is applied at a distance equal to 2/3 of the grouser's height. (Note that this formulation is exact only when α = 0). The total grouser torque is a sum of these individual grouser torques.

The stresses acting over the wheel-terrain contact surfaces are resolved along the normal, longitudinal, and lateral wheel directions, then summed to compute net forces acting on the wheel.

The thrust, *T*, is computed as the sum of all shear force components in the direction of forward wheel motion.

$$T = br\int_{\theta_r}^{\theta_f}\tau\cos\theta\, d\theta \tag{16}$$

Compaction resistance, R_c, is the result of all normal force components acting to resist forward motion.

$$R_c = br \int_{\theta_r}^{\theta_f} \sigma \sin\theta \, d\theta \tag{17}$$

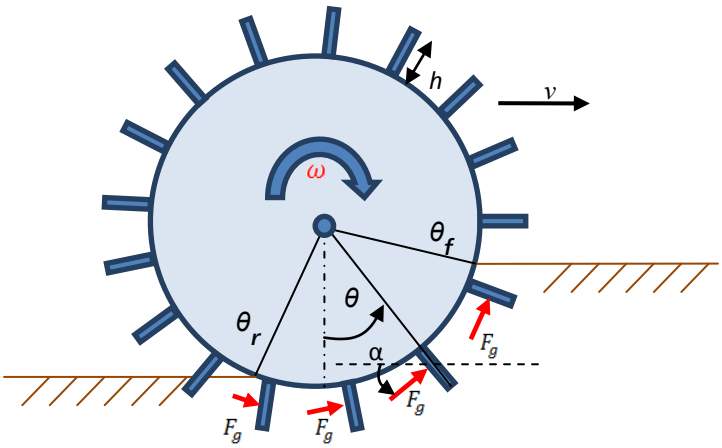

Figure 3: Tractive forces due to wheel grousers (cleats)

Drawbar pull, *DP*, is calculated as the net longitudinal force (i.e. the difference between the thrust force and resistance force). *DP* is the resultant force that can either accelerate the wheel or provide a pulling force at the vehicle axle.

$$DP = T - R_c + F_g \tag{18}$$

The lateral force, *L*, is computed as the combination of lateral shear forces acting at the wheel-terrain interface, F_u, and lateral bulldozing forces acting on the wheel sidewall, F_b.

$$L = F_u + F_b \sin\beta \tag{19}$$

The sum of forces in the normal direction results in the normal force *W*, which balances the weight of the rover in the absence of inertial forces.

$$W = br \int_{\theta_r}^{\theta_f} (\sigma \cos\theta + \tau \sin\theta) d\theta + \sum F_g \sin\theta \tag{20}$$

2.2 Slip Modeling

Determination of a wheel's slip or skid state is required for calculation of the force relations presented above. The value of slip or slid, *i*, is bounded from -100% to 100%. Definitions for slip (driving) and skid (braking) are given in Equation 21.

$$i = \begin{cases} 1 - \frac{v}{r\omega} & (if \;\; v < r\omega \; driving) \\ \\ \frac{r\omega}{v} - 1 & (if \;\; v > r\omega \; braking) \end{cases} \tag{21}$$

Wheel slip often results in excavation of soil around the wheel, leading to downward wheel displacement termed slip sinkage. ARTEMIS employs a model from [18] for slip sinkage. The amount of slip sinkage is controlled by modifying a soil exponent index, which modulates the soil pressures in Equation 1.

$$n = n_0 + n_1 |i| \tag{22}$$

2.3 Case Study: Opportunity Drive to Endeavor Crater

Here the results from a case study simulation with ARTEMIS are presented. This case study focuses on

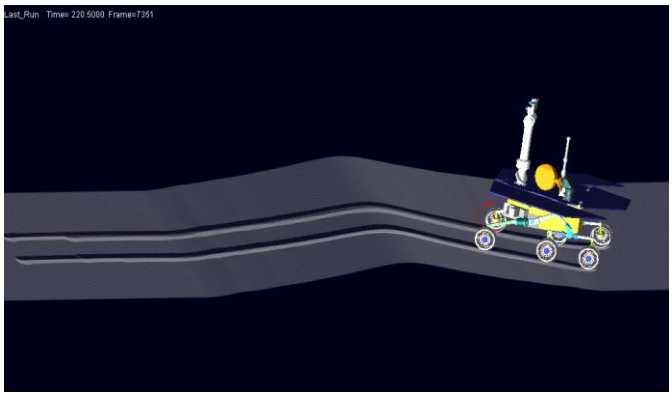

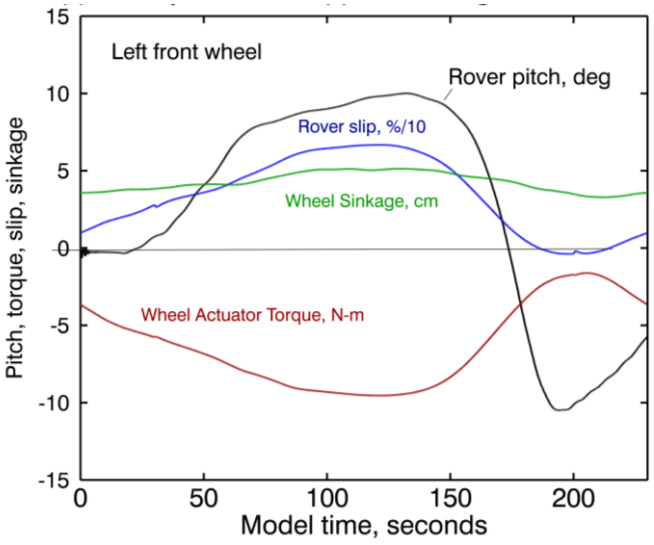

Figure 4: Left panel shows the rover model with tracks produced, noting that the rover drove backwards. Right panel shows plots of rover pitch with positive values indicating that the front of the rover was pointing downhill relative to the local gravity vector. Note the increased left front wheel torques and sinkage, and the slippage estimates as the rover ascended the ripple flank.

simulating events that took place during the Opportunity rover's activities on sol (Mars day) 2143, when the rover crossed a 5 m wide, 0.5 m high wind-blown ripple dominated by relatively loose, poorly sorted basaltic sands. Opportunity was observed to experience significant slippage (up to 65%) and sinkage (up to ~5cm) when climbing the western side of ripples, particularly for the downslope wheels.

Figure 4 depicts a time-history of data from a simulation of Opportunity crossing the ripple, using a digital elevation map derived from Navigation Camera (Navcam) stereo images acquired post-crossing. In this simulation, terrain parameters were chosen for their similarity to consolidated, poorly sorted sands. Data are plotted for the right-front rover wheels, and include wheel slip, torque, and sinkage as a function of time. Rover pitch is also presented. Note that Opportunity drives backwards over the ripple, and thus the front wheels were located on the downslope side as the vehicle proceeded up the ripple flank.

The simulation results show that increased wheel sinkage due to increased weight over a given wheel led to increased compaction resistance. This caused increased slippage for a driven wheel. As slippage increased, additional sinkage occurred due to the skip sinkage effect. This further increased motion resistance. The results presented in Figure 4 were found to be similar to observed experimental data, thus providing a coarse validation of the overall modeling approach.

Additional case studies have been performed involving the Spirit rover. Simulations were performed that replicated yaw motion about the rover's inoperable right-front wheel, translational movement down slopes, excessive (~90%) slip while driving, and a tendency to "pop a wheelie" with the right middle wheel during certain drive events.

Current work is focused on optimization of ARTEMIS runtime speed, and modeling of multipass effects. Other topics of interest involve developing parallelized implementations of ARTEMIS, to enable efficient stochastic simulation. Validation of model results is also underway using a simulation of a single rover wheel to compare to laboratory single-wheel testbed data and tests on soil-covered surfaces at JPL using the engineering version of the MER rovers.

3.0 ESTIMATION OF TERRAIN MODEL PARAMETERS FROM MER ROVER TELEMETRY

The wheel-terrain interaction models presented earlier in this paper rely on terrain-specific parameters. These parameters must be correctly estimated in order to accurately predict rover mobility. In classical terramechanics approaches, six parameters are necessary to characterize the terrain:

- cohesion, c
- angle of internal friction, ϕ
- cohesion dependent parameter, k_c
- friction angle dependent parameter, k_ϕ
- sinkage exponent, n
- shear modulus, k_x

To obtain these parameters it is typically necessary to conduct at least two types of tests: a series of direct shear tests to estimate c, ϕ, and k_x, and a series of bevameter tests to estimate k_c, k_ϕ, and n. However, since these tests must be performed on physical soil samples (which are not available for Mars regolith), other estimation methods must be adopted.

Here a soil parameter estimation procedure based on constrained optimization is introduced that merges a Bekker/Wong wheel-terrain interaction model and telemetry data acquired during Mars Exploration Rover mission operation. Note that Sullivan [19] has previously estimated Mars soil parameters via wheel trenching and scuffing experiments, however these experiments focused on estimating soil cohesion and angle of internal friction, and not Bekker parameters (k_c, k_ϕ, and n). The proposed approach can thus be viewed as complementary to the work presented in [19].

3.1 Parameter Estimation Problem Statement

The parameter estimation problem can be stated as follows. Consider a physical process where a set of variables y is assumed to be related to independent variables x and unknown parameters θ through:

$$y = f(x, \theta) \tag{23}$$

If a series of n observations are available, then for n values of x a corresponding n values of y are measured. For each observation μ it is possible to define a vector of residuals e_μ:

$$e_\mu(\theta) = y_\mu - f(x_\mu, \theta) \tag{24}$$

The second moment matrix of the residuals is derived as follows:

$$M(\theta) = \sum_{\mu=1}^{n} e_\mu(\theta) e_\mu^T(\theta) \tag{25}$$

The unknown parameters θ can be estimated by minimizing some objective function. The objective function is defined by the user, and its selection depends on the goal of the optimization. Common approaches include least squares, maximum likelihood, and Bayesian estimation. Here, the least square methodology is adopted. The objective function is then:

$$\Phi(\theta) = Tr(M(\theta)) \tag{26}$$

Minimization of Equation 26 can be achieved through various methodologies, including gradient methods and genetic algorithms. Here the classical Levenberg-Marquardt gradient method was used.

3.2 Model and Assumptions

It is assumed that the soil parameters introduced in Section 3.0 are the sole terrain parameters of interest in the estimation problem. Estimation of other model parameters introduced in

Section 2 is not addressed here. Knowedge of the rover pose and driving torque applied to each wheel is available from telemetry, while slip and sinkage can be derived from telemetry data. It is also assumed that the rover is moving slowly, and thus dynamic load transfer among rover wheels is negligible. Finally, it is assumed that the rover kinematics and mass properties are precisely known. This assumption is reasonable, since extensive characterization of the rover was performed before flight.

The semi-empirical wheel-terrain interaction model used for parameter estimation bears close similarity to the model employed in ARTEMIS. A modeling methodology based on the work of Bekker [10] and Wong and Reece [12,13], is adopted. This model is valid for rigid wheels interacting with deformable terrain. The first step for a semi-empirical method is to estimate the stress distribution along the contact patch. Both normal and shear stresses develop at the interface between a rotating wheel and the soil surface.

The normal stress is calculated from pressure-sinkage equations described in Equation 1. The calculation of shear stress beneath the wheel is based upon an empirical expression first introduced by Janosi and Hanamoto [14] and described in Equation 3. It should be noted that the terrain below a rolling tire is under a complex stress state, which is theoretically not properly represented by the Mohr-Coulomb failure criterion.

As in the ARTEMIS model, the location of the maximum stress is taken to be a linear function of the slip ratio and the entry angle, as described in Equation 2. The value of the terrain exit angle θ_r is here taken to be zero. This implicitly assumes that the terrain is perfectly plastic. Inspection of MER rover Navcam imagery, which in some cases provides a view of the exit angle, has shown this to be a reasonable assumption.

Given the normal and tangential stress distributions, it is possible to calculate the drawbar pull and driving torque. The balance of vertical forces must first be calculated, since it ensures that the vertical force produced along the contact patch balances the vertical load on the wheel. Here, the vertical load on a given wheel is computed under the assumption that dynamic effects are negligible (i.e. the quasi-static assumption). Then, given knowledge of the rover mass and center of gravity position, rover telemetry data describing the pose is sufficent to compute the load on a given wheel.

Telemetry can also be used to compute the driving torque exerted on the front two rover wheels. These two wheels (out of six total wheels) were instrumented with thermocouples to measure the motor operating temperature. This measurement is required to estimate the applied torque, since torque was shown to exhibit a strong dependence on temperature in pre-flight testing [20].

Wheel sinkage can be measured by analyzing MER rover Navcam imagery. Navcam images often provide clear views of the ruts left by rover passage in deformable soil. Stereo image analysis can provide accurate measurement of the depth of these ruts, thus providing wheel sinkage estimates that can be registered to a specific location. It should be noted that this measured sinkage represents the combined effects of three wheels passing over the same patch of terrain, and thus multi-pass effects should be considered. Current efforts are aimed at developing methods to estimate multi-pass model parameters.

Wheel slip can be measured in one of two ways. The first is by analyzing MER rover Navcam imagery. The MER rover wheels possess features to enable rigid mounting to the lander platform, to ensure rover stability during flight, and atmospheric entry, descent, and landing. When a MER rover wheel is driven over deformable soil, these “tie down” features yield distinct marks in the soil. The distance between these marks can be precisely measured from stereo Navcam imagery, and represent the actual distance traveled during one complete wheel revolution. By comparing this actual distance to the estimated distance (measured from wheel odometry), an average value of wheel slip can be calculated over a single wheel revolution.

The second way to measure wheel slip is by employing visual odometry [21]. Visual odometry is a method for estimating absolute vehicle motion, including individual wheel motion, based on measured diplacements of visual features in successive image frames and knowledge of the rover kinematic properties. While visual odometry may provide a more precise measure of individual wheel slip, is was not operational at all times on the MER rovers due to its computational cost.

3.3 Parameter Estimation Case Study and Discussion

To perform parameter estimation, wheel torque, thrust, and sinkage predicted by the wheel-terrain interaction model are compared with values measured or extracted from robot telemetry. A vector of unknown terrain parameters is varied such that the squared summation of the residuals e_μ is minimized. The process is illustrated in Figure 5.

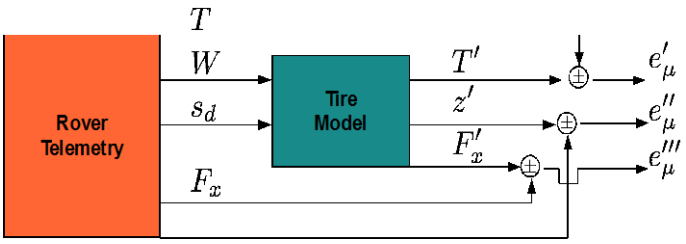

Figure 5: Schematic representation of the parameter estimation methodology. Acceptable parameters are the ones that minimize the residuals e_μ

A simulation-based case study has been performed by generating a series of observations from randomly sampled vertical load and slip ratios, based on a set of soil parameters that are typical for dry sand (see Table 1). For every value of W and s_d a corresponding value of torque T and thrust F_x are generated. Soil parameters are then perturbed, and the least squares approach is used to find soil parameters that minimize the residuals between T and F_x and the calculated values T' and F_x'. The input vertical load and slip ratio are assumed to be known accurately (i.e., the randomly generated W and s_d adopted to create the sample observations are also used as inputs to the wheel-soil interaction model).

Table 1: Soil properties adopted in case study (from Wong [10])

Soil	k_c $\left[\frac{\text{kN}}{\text{m}^{n+1}}\right]$	k_ϕ $\left[\frac{\text{kN}}{\text{m}^{n+2}}\right]$	n	c [Pa]	ϕ [deg]	k_x [m]
Dry Sand	6.94	505.8	0.705	960	27.3	0.0114

The wheel-soil interaction equations are non linear integral equations. This leads to the problem of non uniqueness of the solution: there are several sets of parameters that can be found that (locally) minimize Equation 26. This problem can theoretically be mitigated by increasing the number of observations, however such an approach does not guarantee improvement of the estimation accuracy. To reduce the order of the problem, an attempt to condense the Bekker parameters into a single constant has been pursued. The Bekker pressure-sinkage equation has been modified as follows:

$$\sigma = k_{bekker}\left(\frac{z}{b}\right)^n \tag{27}$$

This formulation reduces the number of parameters since k_c and k_ϕ are reduced to a single parameter, k_{bekker}. This assumption is justified by the fact that k_c and k_ϕ are only loosely related to inherent terrain physical properties, and instead are empirical parameters that can vary greatly depending on testing conditions.

Figure 6 presents results for parameter estimation assuming a single Bekker constant. The parameters are initially perturbed by 49% (i.e. the initial guess differed from the true parameters by 49%). It can be seen that the number of observations does not appear to have a strong impact on the accuracy of the estimation. This is likely due to the non uniqueness issue mentioned previously. The sinkage exponent n is estimated relatively accurately, and the angle of internal friction ϕ, the Bekker constant k_{bekker} and the shear modulus k_x are bounded by ±10%. The soil cohesion c does not follow a clear trend. This is due to the fact that the wheel-terrain interaction model is more sensitive to certain parameters than others. Moreover, sand is a poorly cohesive soil, and thus the influence of cohesion is very weak.

This case study suggests that the proposed approach to Mars terrain parameter estimation represents a credible method for estimating the physical properties of Mars soil, given prior knowledge of various rover physical properties and information derived from rover telemetry. Preliminary analysis of MER Opportunity rover telemetry from sol 2143 has suggested that it is possible to apply the parameter estimation approach to actual Mars rover telemetry. Analysis of additional telemetry data, and characterization of estimation uncertainty, are topics of current research.

4.0 CURRENT RESEARCH DIRECTIONS

The ARTEMIS rover simulation tool is one of several complementary methods currently being developed by the authors to improve the ability to plan safe rover operations on sloped and deformable terrain. Other simulation efforts include modeling of rover-soil interaction using discrete element methods. Such an approach is expected to be valuable in scenarios where the rover is deeply embedded in soil. In such cases, classical Bekker-Wong models have not been validated.

Another method under development will correlate rover telemetry to observables from orbiting sensors to enable prediction of rover performance over broad spatial areas. This method will rely on machine learning methods to yield predictions that will help engineers make decisions related to large-scale rover drive strategies.

Lastly, efforts are underway to develop classification-based strategies to detect instances of high wheel slip and sinkage, based on on-board analysis rover sensor data. Similar approaches have been developed by the authors for terrestrial mobile robots, with a high degree of success [22].

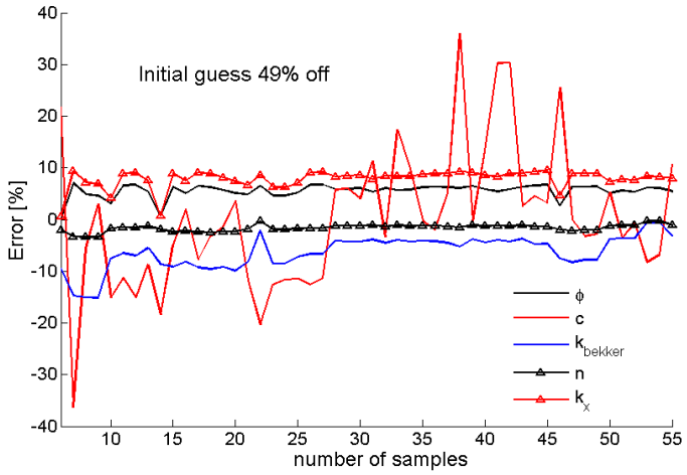

Figure 6: Parameter estimation error trend vs number of samples employed in estimation. The initial guess differs from the true parameter values by 49%.

ACKNOWLEDGMENTS

The authors would like to thank Scott Maxwell of JPL for his valuable insight into MER rover operational procedures and rover drive behavior.

REFERENCES

[1] Mishkin, A., Morrison, J., Nguyen, T., Stone, H., Cooper, B., and Wilcox, B., "Experiences with operations and autonomy of the Mars Pathfinder Micro-Rover," *Proceedings of the 1998 IEEE Aerospace Conference*, pp. 337 – 351, 1998.

[2] Arvidson, R. E., et al. "Spirit Mars Rover mission to the Columbia Hills, Gusev Crater: Mission overview and selected results from the Cumberland Ridge to Home Plate," *Journal of Geophysical Research—Planets*, Vol. 113, E12S33, doi:10.1029/ 2008JE003183, 2008.

[3] Arvidson, R. E., et al. "Spirit Mars Rover mission: Overview and selected results from the northern Home Plate Winter Haven to the side of Scamander crater,"

Journal of Geophysical Research—Planets, Vol. 115, E00F03, doi:10.1029/ 2010JE003633, 2010.

[4] Arvidson, R., et al., "Opportunity Mars Rover Mission: Overview and Selected Results from Purgatory Ripple to Traverses to Endeavour Crater," *Journal of Geophysical Research—Planets*, Vol. 116, E00F15, doi:10.1029/ 2010JE003746, 2011.

[5] Trease, B., Arvidson, R., Lindemann, R., Bennett, K., Zhou, F., Iagnemma, K., Senatore, C., VanDyke, L., "Dynamic modeling and soil mechanics for path planning of Mars exploration rovers," *Proceedings of the ASME Design Engineering Technical Conference*, 2011.

[6] Iagnemma, K., Kang, S., Shibly, H., and Dubowsky, S.,, "On-Line terrain parameter estimation for planetary rovers," *IEEE Transactions on Robotics and Automation*, Vol. 20, Number 5, pp. 921-927, October 2004.

[7] Hutangkabodee, S., Zweiri, Y., Seneviratne, L., and Althoefer, K., "Soil parameter identification for wheel-terrain interaction dynamics and traversability prediction," *International Journal of Automation and Computing*, Vol. 3, No. 3, pp. 244-251, 2006.

[8] Ojeda, L., Borenstein, J., Witus, G., and Karlsen, R., "Terrain Characterization and Classification with a Mobile Robot, *Journal of Field Robotics*, Vol. 23, No. 2: 103-122, 2006.

[9] Ray, L. "Autonomous terrain parameter estimation for wheeled vehicles," *Proceedings of the SPIE Conference on Unmanned Systems Technology*, 2008.

[10] Bekker, M. G., *Theory of land locomotion: The mechanics of vehicle mobility*, The University of Michigan Press, Ann Arbor, 1956.

[11] Wong, J. Y., *Terramechanics and Off-Road Vehicle Engineering*, 2nd Ed., Elsevier, 2010

[12] Wong, J. Y., "Prediction of rigid wheel performance based on the analysis of soil-wheel stresses part I," *Journal of Terramechanics*, Vol. 4, No. 1, pp. 81-98, 1967.

[13] Wong, J. Y., "Prediction of rigid wheel performance based on the analysis of soil-wheel stresses part II," *Journal of Terramechanics*, Vol. 4, No. 2, pp. 7-25, 1967.

[14] Janosi, Z., and Hanamoto, B., "Analytical determination of drawbar pull as a function of slip for tracked vehicles in deformable soils," *Proceedings of the 1st International Conference on Terrain-Vehicle Systems*, Turin, Italy, 1967.

[15] Ishigami, G., Miwa, A., Nagatani, K., Yoshida, K., "Terramechanics-based model for steering maneuver of planetary exploration rovers on loose soil," *Journal of Field robotics*, Vol. 24, No. 3, 233-250, 2007.

[16] Schwanghart, H., "Lateral forces on steered tyres in loose soil," *Journal of Terramechanics*, 1(1):9-29, 1968.

[17] Terzaghi, K., Peck, R. B., and Mesri, G., *Soil mechanics in Engineering Practice*, John Wiley & Sons, New York, 3rd edition, 1996.

[18] Ding, L., Gao, H., Deng, Z., Tao, J., "Wheel slip-sinkage and its prediction model of lunar rover," *Journal of Center South University Technology*, Vol. 17, pp. 129-135, 2010.

[19] Sullivan, R., Anderson, R., Biesiadecki, J., Bond, T., and Stewart, H., "Cohesions, friction angles, and other physical properties of Martian regolith from Mars Exploration Rover wheel trenches and wheel scuffs", *Journal of Geophysical Research*, Vol. 116, E02006, 38 pp., 2011.

[20] Lindemann R., "Dynamic testing and simulation of the Mars exploration rover," *Proceedings of ASME International Design Engineering Technical Conferences*, pp. 99-106, 2005.

[21] Maimone, M., Cheng, Y., Matthies, L., "Two Years of visual odometry on the Mars exploration rovers," *Journal of Field Robotics*, Vol. 24, No. 3, pp. 169-186, 2007.

[22] Iagnemma, K., and Ward, C., "Classification-based wheel slip detection and detector fusion for mobile robots on outdoor terrain," *Autonomous Robots*, Vol. 26, pp. 33-46, January 2009.